ARTICLE IN PRESS

Journal of Computational Physics xxx (2012) xxx–xxx

Contents lists available at SciVerse ScienceDirect

Journal of Computational Physics

journal homepage: www.elsevier.com/locate/jcp

Unified framework for a side-by-side comparison of different multicomponent algorithms: Lattice Boltzmann vs. phase field model

Luca Scarbolo [a,*], Dafne Molin [a,b], Prasad Perlekar [d,e], Mauro Sbragaglia [c], Alfredo Soldati [a], Federico Toschi [d,e]

[a] Dipartimento di Energetica e Macchine, Università degli Studi di Udine, 33100 Udine, Italy
[b] Dipartimento di Ingegneria Meccanica, Università degli Studi di Brescia, 25133 Brescia, Italy
[c] Dipartimento di Fisica and INFN, Università di Roma "Tor Vergata", 00133 Rome, Italy
[d] Department of Applied Physics and Mathematics and Computer Science, Technische Universiteit Eindhoven, P.O. Box 513, 5600 MB Eindhoven, Netherlands
[e] CNR-IAC, Via dei Taurini 19, 00185 Rome, Italy

ARTICLE INFO

Article history:
Received 14 December 2011
Received in revised form 20 September 2012
Accepted 22 September 2012
Available online xxxx

Keywords:
Phase field model
Lattice Boltzmann
Navier–Stokes
Cahn–Hilliard
Comparison
Drop
Leakage
Spurious currents

ABSTRACT

Lattice Boltzmann models (LBM) and phase field models (PFM) are two of the most widespread approaches for the numerical study of multicomponent fluid systems. Both methods have been successfully employed by several authors but, despite their popularity, still remains unclear how to properly compare them and how they perform on the same problem. Here we present a unified framework for the direct (one-to-one) comparison of the multicomponent LBM against the PFM. We provide analytical guidelines on how to compare the Shan–Chen (SC) lattice Boltzmann model for non-ideal multicomponent fluids with a corresponding free energy (FE) lattice Boltzmann model. Then, in order to properly compare the LBM vs. the PFM, we propose a new formulation for the free energy of the Cahn–Hilliard/Navier–Stokes equations. Finally, the LBM model is numerically compared with the corresponding phase field model solved by means of a pseudo-spectral algorithm. This work constitute a first attempt to set the basis for a quantitative comparison between different algorithms for multicomponent fluids. We limit our scope to the few of the most common variants of the two most widespread methodologies, namely the lattice Boltzmann model (SC and FE variants) and the phase field model.

1. Introduction

Since the beginning of the last century several approaches have been developed for theoretical analysis and numerical simulation of multicomponent and multiphase flows. The most common theoretical approach to study such complex systems is based on the sharp-interface assumption, in which the interface between the different fluids is considered of zero-thickness. Each component is characterized by its own physical properties, such as density, concentration, and viscosity which are uniform over the portion of the domain occupied by the single fluid component. These physical properties may change in a discontinuous way across the interface and their jumps are determined by the equilibrium conditions at the interface. The evolution of the system is described by a set of conservation laws (mass, momentum, energy, etc.) separately written for each component. Their solution requires also a set of boundary conditions at the interface, which ultimately has to be tracked. The specific numerical difficulties involved with the interface tracking can be circumvented by the adoption of

* Corresponding author. Tel.: +39 0432 558005.
E-mail addresses: luca.scarbolo@uniud.it (L. Scarbolo), dafne.molin@ing.unibs.it (D. Molin), p.perlekar@tue.nl (P. Perlekar), sbragaglia@roma2.infn.it (M. Sbragaglia), soldati@uniud.it (A. Soldati), f.toschi@tue.nl (F. Toschi).

0021-9991/$ - see front matter © 2012 Elsevier Inc. All rights reserved.
http://dx.doi.org/10.1016/j.jcp.2012.09.029

diffuse interface methods, like the ones focus of the present study: the multicomponent Lattice Boltzmann method (LBM) and the phase field model (PFM). The drawback of these models is the high numerical resolution necessary to model real interface thickness that require a fictitious enlargement of the interface thickness. Despite this limitation, in recent years several researchers worked on the development and refinement of PFM as well as different variants of the multicomponent LBM.

1.1. Introduction to LBM

The kinetic theory for multicomponent fluids and gas mixtures has received a lot of attention in literature [1–7]. Many of the kinetic models developed for the study of mixtures are based on the linearized Boltzmann equations, especially the single-relaxation-time model due to Bhatnagar et al. [8], also named BGK-model:

$$\frac{\partial f(\mathbf{x},\mathbf{v},t)}{\partial t}+\mathbf{v}\cdot\nabla f(\mathbf{x},\mathbf{v},t)+\mathbf{a}\cdot\nabla_{\mathbf{v}}f(\mathbf{x},\mathbf{v},t)=\Omega(\mathbf{x},t)==-\frac{1}{\tau}\left[f(\mathbf{x},\mathbf{v},t)-f^{(eq)}(\mathbf{x},\mathbf{v},t)\right], \tag{1}$$

where $f(\mathbf{x},\mathbf{v},t)$ is the probability density function to find at the space–time location $(\mathbf{x},t)$ a particle with velocity $\mathbf{v}$. The collisional kernel, on the right hand side of Eq. (1), stands for the relaxation (with a characteristic relaxation time τ) towards the local equilibrium $f^{(eq)}(\mathbf{x},\mathbf{v},t)$ which, in turn, depends on the local coarse grained variables, as density and momentum:

$$\rho(\mathbf{x},t)=\int f(\mathbf{x},\mathbf{v},t)\mathrm{d}\mathbf{v}\quad \rho\mathbf{u}(\mathbf{x},t)=\int f(\mathbf{x},\mathbf{v},t)\mathbf{v}\mathrm{d}\mathbf{v}. \tag{2}$$

$\mathbf{a}\cdot\nabla_{\mathbf{v}}f(\mathbf{x},\mathbf{v},t)$ represents the effect of a volume/body force density, $\mathbf{a}$, on the kinetic dynamics. Modern discrete-velocity counterparts of (1), the so-called Lattice Boltzmann methods (LBM), are able to simulate multiphase and multicomponent fluids and have attracted considerable attention from the scientific community [9–18]. The LBM is an discrete form of Boltzmann kinetic equation describing the dynamics of a fictitious ensemble of particles [19–22], whose motion and interactions are confined to a regular space–time lattice. This approach consists in the following evolution:

$$f_i(\mathbf{x}+\mathbf{c}_i\Delta t,t+\Delta t)-f_i(\mathbf{x},t)=-\frac{\Delta t}{\tau}[f_i(\mathbf{x},t)-f_i^{(eq)}(\mathbf{x},t)], \tag{3}$$

where $f_i(\mathbf{x},t)$ is the probability density function of finding a particle at site $\mathbf{x}$ and time t, moving in the direction of the i-th lattice speed $\mathbf{c}_i$ with $i=0,\ldots,b$. Systematic ways to derive the discrete set of velocities in these models are either the discretization of the Boltzmann equation on the roots of Hermite polynomials [23–29] or the construction of high-order lattices for more stable LBM based on entropic approaches [30,31]. At the same time, the translation of the body/volume force $\mathbf{a}\cdot\nabla_{\mathbf{v}}f(\mathbf{x},\mathbf{v},t)$ onto the discrete-lattice framework represented one of the most challenging issues in the last years of Lattice Boltzmann research [11–17,32–36]. Through one of the first approaches proposed in the literature, the so called Shan–Chen (SC) approach [11,12], the non-ideal interactions have been introduced directly at the discrete lattice level among the constituent (kinetic) particles [11,12,37]. These lattice forces embed the essential features and are able to produce phase separation (i.e. a non-ideal equation of state and a non-zero surface tension) as well as a detailed diffuse interface structure. The application of the SC models has been particularly fruitful for many applications [38,36,39–42]. Nevertheless, its theoretical foundations have been object of debate in the recent years [32,37,40,41], mainly because of the thermodynamic consistency of the mesoscopic interactions involved. On the other hand, in the so called free-energy (FE) models [15–17], the collisional properties of the model have been chosen in such a way that the large scale equilibrium is consistent with an underlying free energy functional, embedding both hard core effects and weak interacting tails. In this case, more traceable theoretical foundations have been provided, at least from the point of view of a continuum theory [43]. Among others, some studies have also performed where more elaborated lattice models, including the effect of an exclusion volume based on Enskog theory [32,34,33], effective equilibria [39], or even effective SC forces, were designed to match the desired bulk pressure of a given fluid [35,36].

1.2. Introduction to PFM

The phase field model is based on the idea that the interface between two fluids is a layer of finite thickness rather than a sharp discontinuity. Across the interfacial layer the physical properties of the mixture components vary in a smooth and continuous way, from one fluid to the other. This approach is based on the pioneering work of van der Waals [44], who first determined the interface thickness of a critical liquid–vapor mixture. In the PFM the state of the system is described, at any time, by an order parameter $\phi=\phi(\mathbf{x})$, which is a function of the position vector $\mathbf{x}$. The order parameter directly represents a physical properties of the fluid, such as its density, molar concentration, etc.; all the remaining properties are in turn modeled as proportional to $\phi(\mathbf{x})$ [45,46]. According to the diffuse-interface approach, the order parameter is continuous over the entire domain and it shows smooth variations across the interface between single fluid regions, where $\phi(\mathbf{x})$ assumes approximately uniform values. Coupling the continuous and diffuse representation of the system with a transport equation of the order parameter, the system evolution can be resolved in time. One of the best-known PFM is the Cahn–Hilliard equation [47,48], an extension to binary mixtures of the work of van der Waals [44]. This equation is a transport equation

Please cite this article in press as: L. Scarbolo et al., Unified framework for a side-by-side comparison of different multicomponent algorithms: Lattice Boltzmann vs. phase field model, J. Comput. Phys. (2012), http://dx.doi.org/10.1016/j.jcp.2012.09.029

for the order parameter, where the evolution of $\phi(\mathbf{x})$ is proportional to the gradient of the chemical potential, μ. The chemical potential is defined in terms of the free energy functional, $\mathcal{F}[\phi]$:

$$\mu = \frac{\delta \mathcal{F}[\phi]}{\delta \phi}, \tag{4}$$

where the free energy, $\mathcal{F}[\phi]$, assumes suitable definitions according to the problem under analysis (and also depending on which physical quantity has to be described) and is a conservative, thermodynamically consistent functional. The most common free energy formulation is given by the sum of an ideal part, $\mathcal{F}_{id}[\phi]$, and a non-local part, $\mathcal{F}_{nl}[\nabla\phi]$. The ideal part accounts for the tendency of the system to separate in two pure components and is derived from the thermodynamics of mixtures. The non-local part accounts for the diffusive interfacial region. Through the Cahn–Hilliard equation, the evolution of the order parameter is thermodynamically consistent and subject to a phase field conservation. As a result, the prediction of the interfacial layer does not deteriorate. In the case of density-matched fluid systems, the convective Cahn–Hilliard equation is coupled with a modified Navier–Stokes equation, where a surface tension (or capillary) forcing term, which is derived from the Korteweg stress [49], is introduced. This contribution yields to the Cahn–Hilliard/Navier–Stokes coupled equations system [50–52], which is also known as Model-H, according to the classification of Hohenberg and Halperin [53], who studied the convective phase separation of a partially miscible fluid mixture. This model, originally developed to study critical phenomena [54–58], was subsequently used by many authors to study two-phase flows of Newtonian fluids [59,50,60,46,61]. In this case, even if the fluids are in fact immiscible, molecular diffusion between the two species is allowed in the interfacial region. Thus, the thinner is the interface, the more realistic is the numerical solution. Realistic interface thickness requires high numerical resolution, which is usually beyond current computational limits. For this reason the interface is often kept larger than corresponding physical value (this approximation holds also for lattice Boltzmann approaches). However, in spite of this approximation, the method has shown capabilities to capture complex interfacial dynamics in a wide range of real physical problems [45,50,62,63].

1.3. Advantages and disadvantages of the methods

Multicomponent LBM and PFM have demonstrated excellent performances to predict the dynamics of multiphase and multicomponent flows. Yet, both methods show their own peculiar characteristics and drawbacks which can limit their use, performances and range of validity. A particular unexpected, and unwanted, feature of multiphase and multicomponent solvers is the manifestation of non physical velocities near equilibrium interface, present even for systems at rest. From a physical viewpoint the velocity should clearly vanish at equilibrium but, as it has been observed by many authors, small spurious currents most often exist in the proximity of the interfaces. In an attempt to remove these unwanted features several improvement to the LBM have been proposed in recent years [64–69]. It worths noticing that some of these improvement are capable to remove these spurious current to machine precision [67]. Spurious currents have also been observed in other numerical methods including the PFM [70–72].

Because of the magnitude of these spurious current drastically depend on the actual variant of the LBM or PFM, the comparison between the two methods may be somewhat ill defined. Here we aim at comparing the LBM vs. the PFM for their most widespread and used variants. Our answer will thus not provide a general statement valid for the two methods as such, but will still provide some extremely useful insight in what can be expected from the most employed variations of the approaches. As a side results, we will also quantitatively compare two of the most widely used lattice Boltzmann variants, the SC-LBM and the FE-LBM, under the same conditions (i.e. same diffuse interface model, same surface tension, same chemical potential, etc.). In order to achieve our goal, the problem of a one-to-one matching of the PFM with SC/FE multicomponent LBM needs to be addressed first. The one-to-one matching of the two methods gives also the opportunity to clarify how they compare with respect to the computational costs. In order to address these issues we start by analyzing the SC model for two population with inter-particle repulsion; the large scale continuum limit is reviewed and formulated in terms of a diffuse interface model with an underlying thermodynamic FE functional. In this way one of the crucial issues in the matching of SC model vs. the corresponding FE model is being solved. Then, starting from the matched SC/FE multicomponent LBM, a new formulation for the free-energy of the PFM is derived in order to directly compare them. Finally, a comparison of the numerical results obtained, on the same problem, from both LBM and PFM is presented, focusing in particular on unwanted spurious currents or mass leakage in sheared suspensions. This work focuses only the case of binary mixtures, even if modeling more than two components is nowadays far from trial extension [73–77].

2. The lattice Boltzmann models

2.1. The multicomponent Shan–Chen model

In this section the multicomponent model introduced by Shan & Chen [11,12] is reviewed. First the main properties of the model are recalled, then the equilibrium features (diffusive current and pressure tensor) relevant on the hydrodynamic scales are analyzed. Starting from a kinetic lattice Boltzmann equation [19,20,22] for a multicomponent fluid with N_s species [13,14], the evolution equations over a characteristic time lapse Δt read as follows:

Please cite this article in press as: L. Scarbolo et al., Unified framework for a side-by-side comparison of different multicomponent algorithms: Lattice Boltzmann vs. phase field model, J. Comput. Phys. (2012), http://dx.doi.org/10.1016/j.jcp.2012.09.029

$$f_{is}(\mathbf{x}+\mathbf{c}_i\Delta t, t+\Delta t) - f_{is}(\mathbf{x},t) = -\frac{\Delta t}{\tau_s}[f_{is}(\mathbf{x},t) - f_{is}^{(eq)}(\rho_s, \mathbf{u}+\tau_s\mathbf{F}_s/\rho_s)], \tag{5}$$

where $f_{is}(\mathbf{x},t)$ is the probability density function of finding a particle of species $s = 1,\ldots,N_s$. For the sake of simplicity, the characteristic time interval Δt is assumed to be unity in what follows. The left hand-side of (5) accounts for the molecular free-streaming, whereas the right-hand side represents the time relaxation (due to collisions) towards local Maxwellian equilibrium $f_{is}^{(eq)}(\rho_s,\mathbf{u})$ on a time scale τ_s [19,22,20,8]. The local Maxwellian is truncated at second order, leading to a sufficiently accurate approximation to correctly recover the hydrodynamic balance of an isothermal regime [19–22]. It should be noted that the equilibrium for the s species is a function of their local densities and common velocities, defined as:

$$\rho_s(\mathbf{x},t) = \sum_i f_{is}(\mathbf{x},t); \mathbf{u}(\mathbf{x},t) = \frac{\sum_s \frac{1}{\tau_s}\sum_i f_{is}(\mathbf{x},t)\mathbf{c}_i}{\sum_s \frac{1}{\tau_s}\rho_s(\mathbf{x},t)}. \tag{6}$$

This common velocity receives a suitable shift from the force, $\mathbf{F}_s$, acting on the s species [11,13]. $\mathbf{F}_s$ may be either an external force or an internal force representing an intermolecular interactions:

$$\mathbf{F}_s(\mathbf{x},t) = -G_{ss\prime}\rho_s(\mathbf{x},t)\sum_{s\prime\neq s}\sum_i w_i^{(eq)}\rho_{s\prime}(\mathbf{x}+\mathbf{c}_i,t)\mathbf{c}_i, \tag{7}$$

where $w_i^{(eq)}$ are suitable weights used to enforce isotropy of the resulting hydrodynamics [19,20,22]. The weights, $w_i^{(eq)}$, are normalized as follows:

$$\sum_i w_i^{(eq)} c_i^a c_j^b = \delta_{ab} c_S^2, \tag{8}$$

$$\sum_i w_i^{(eq)} c_i^a c_i^b c_i^s c_i^k = c_S^4(\delta_{ab}\delta_{sk} + \delta_{ak}\delta_{bs} + \delta_{as}\delta_{bk}), \tag{9}$$

where δ_{ab} is the Kronecker delta and $c_S^2 = 1/3$ a constant. In the long-wavelength limit (i.e. when the fluctuations with respect to the equilibrium distribution function are small) the set of macroscopic equations associated with the kinetic model consist of the continuity equations (one for each component) and of the equation of motion for the total fluid momentum. Dealing with the two species (i.e. A and B) under the assumption of the same characteristic time scale for all the components $\tau_s = \tau$,[1] these equations are approximated by:

$$\frac{\partial\rho_s}{\partial t} + \nabla\cdot(\rho_s\mathbf{u}) = \nabla\cdot\mathbf{J}^{(s)}, \tag{10}$$

$$\rho\left(\frac{\partial\mathbf{u}}{\partial t} + \mathbf{u}\cdot\nabla\mathbf{u}\right) = -\nabla\cdot\mathbf{P} + \nabla\cdot(\eta(\tau)\nabla\mathbf{u} + \eta(\tau)\nabla\mathbf{u}^T), \tag{11}$$

where $\rho = \sum_s\rho_s$ is the total density, $\mathbf{u} = \sum_s\rho_s\mathbf{u}_s/\rho$ is the baricentric (total) fluid velocity and $\mathbf{P}$ the pressure tensor with the property $-\nabla\cdot\mathbf{P} + \nabla(c_S^2\rho) = \sum_s\mathbf{F}$. The kinematic viscosity is $\nu(\tau) = c_S^2(\tau - 1/2)$ and the dynamic viscosity is $\eta(\tau) = \rho\nu(\tau)$. The diffusive current, $\mathbf{J}^{(s)}$, is given by the following:

$$\mathbf{J}^{(A)} = \frac{\rho_A\rho_B}{\rho}\left[c_S^2\left(\tau-\frac{1}{2}\right)\left(\frac{\nabla\rho_A}{\rho_A} - \frac{\nabla\rho_B}{\rho_B}\right) - \tau\left(\frac{\mathbf{F}^{(\mathbf{A})}}{\rho_A} - \frac{\mathbf{F}^{(\mathbf{B})}}{\rho_B}\right)\right] = -\mathbf{J}^{(B)}, \tag{12}$$

and, for purely repulsive fluids, $\mathbf{F}^{(A,B)}/\rho_{A,B}$ yields:

$$\frac{\mathbf{F}^{(A,B)}}{\rho_{A,B}} = -g_{AB}c_S^2\nabla\rho_{B,A} - \frac{g_{AB}}{2}c_S^2\nabla\Delta\rho_{B,A} + \cdots, \tag{13}$$

where the coupling constant $G_{ss\prime} = g_{AB} > 0$. Both continuity equations may be subtracted, obtaining:

$$\frac{\partial\phi}{\partial t} + \nabla\cdot(\phi\mathbf{u}) = \nabla\cdot\mathbf{J}^{(\phi)}, \tag{14}$$

where $\phi = \rho_A - \rho_B$ and where $\mathbf{J}^{(\phi)} = 2\mathbf{J}^{(A)}$. The pressure tensor in the (global) momentum equation is:

$$\mathbf{P} = c_s^2\left[(\rho_A+\rho_B) + g_{AB}\rho_A\rho_B + c_S^2\frac{g_{AB}}{2}\rho_A\Delta\rho_B + c_S^2\frac{g_{AB}}{2}\rho_B\Delta\rho_A\right]\boldsymbol{\delta} + (\nabla\rho_A\cdot\nabla\rho_B)\boldsymbol{\delta} - c_S^4 g_{AB}\nabla\rho_A\nabla\rho_B + \mathbf{K}^{(\tau)}, \tag{15}$$

where the extra spurious τ-dependent contribution $\mathbf{K}^{(\tau)}$ is small for τ close to $1/2$. Its exact expression is reported in [42] and, for the sake of simplicity, it will be neglected by setting τ close to $1/2$, thus $\mathbf{K}^{(\tau)} \to 0$. Summarizing, the following equations system is found:

[1] Whenever timescales are different, the characteristic time maps directly onto an effective relaxation time. For the two species system (A,B) this assumes the form $\bar{\tau} = \frac{\rho_A\tau_A+\rho_B\tau_B}{\rho}$; similar expressions need to be used in the total baricentric velocity.

Please cite this article in press as: L. Scarbolo et al., Unified framework for a side-by-side comparison of different multicomponent algorithms: Lattice Boltzmann vs. phase field model, J. Comput. Phys. (2012), http://dx.doi.org/10.1016/j.jcp.2012.09.029

$$\mathbf{J}^{(\phi)} = \frac{2\rho_A\rho_B c_S^2}{\rho}\left(\tau-\frac{1}{2}\right)\left(\frac{\nabla\rho_A}{\rho_A}-\frac{\nabla\rho_B}{\rho_B}\right) - \frac{2\rho_A\rho_B\tau}{\rho}\left[g_{AB}c_S^2\nabla(\rho_B-\rho_A)+\frac{g_{AB}}{2}c_S^2\nabla\Delta(\rho_B-\rho_A)\right], \tag{16}$$

$$\mathbf{P} = c_s^2\left[(\rho_A+\rho_B)+g_{AB}\rho_A\rho_B+c_S^2\frac{g_{AB}}{2}\rho_A\Delta\rho_B+c_S^2\frac{g_{AB}}{2}\rho_B\Delta\rho_A\right]\boldsymbol{\delta}+(\nabla\rho_A\cdot\nabla\rho_B)\boldsymbol{\delta}-c_S^4 g_{AB}\nabla\rho_A\nabla\rho_B. \tag{17}$$

The variables $\rho=\rho_A+\rho_B$ and $\phi=\rho_A-\rho_B$ can be introduced such as $\rho_A=(\rho+\phi)/2$ and $\rho_B=(\rho-\phi)/2$. Under the assumption of an incompressible fluid at constant ρ, the derivative with respect to the density can be neglected in the pressure tensor:

$$\mathbf{P} = c_s^2\left[\rho+\frac{g_{AB}}{4}(\rho^2-\phi^2)-c_S^2\frac{g_{AB}}{4}\phi\Delta\phi-c_s^2\frac{g_{AB}}{8}|\nabla\phi|^2\right]\boldsymbol{\delta}+c_s^4\frac{g_{AB}}{4}\nabla\phi\nabla\phi, \tag{18}$$

while the diffusive current is mapped into the following expression:

$$\mathbf{J}^{(\phi)} = c_S^2\frac{2\rho_A\rho_B}{\rho}\left(\tau-\frac{1}{2}\right)\left[\nabla\log\left(\frac{\rho+\phi}{\rho-\phi}\right)-g_{AB}^{(\tau)}\nabla\phi-\frac{g_{AB}^{(\tau)}}{2}c_S^2\nabla\Delta\phi\right], \tag{19}$$

or, in a more compact form:

$$\mathbf{J}^{(\phi)} = M(\phi)\left[\frac{c_S^2}{2}\nabla\log\left(\frac{\rho+\phi}{\rho-\phi}\right)-\frac{g_{AB}^{(\tau)}}{2}c_S^2\nabla\phi-\frac{g_{AB}^{(\tau)}}{4}c_S^4\nabla\Delta\phi\right] = M(\phi)\nabla\mu(\phi). \tag{20}$$

Into the equation above, the density-dependent mobility has been introduced:

$$M(\phi) = \frac{4\rho_A\rho_B}{\rho}\left(\tau-\frac{1}{2}\right) = \frac{(\rho^2-\phi^2)}{\rho}\left(\tau-\frac{1}{2}\right), \tag{21}$$

and the chemical potential yields:

$$\mu^{(\tau)}(\phi) = \frac{c_S^2}{2}\log\left(\frac{\rho+\phi}{\rho-\phi}\right)-\frac{g_{AB}^{(\tau)}}{2}c_S^2\phi-\frac{g_{AB}^{(\tau)}}{4}c_S^4\Delta\phi, \tag{22}$$

where the modified (through the relaxation time τ) coupling constant reads:

$$g_{AB}^{(\tau)} = \frac{\tau}{(\tau-\frac{1}{2})}g_{AB}, \tag{23}$$

which reduces to g_{AB} in the limit $\tau\gg 1/2$. Summarizing, the set of incompressible equations which are approximated on a large scale are given by

$$\frac{\partial\phi}{\partial t}+\nabla\cdot(\phi\mathbf{u}) = \nabla\cdot\mathbf{J}^{(\phi)}, \tag{24}$$

$$\rho\left(\frac{\partial\mathbf{u}}{\partial t}+\mathbf{u}\cdot\nabla\mathbf{u}\right) = -\nabla\cdot\mathbf{P}+\nabla\cdot(\eta(\tau)\nabla\mathbf{u}+\eta(\tau)\nabla\mathbf{u}^T), \tag{25}$$

where $\mathbf{P}$ and $\mathbf{J}^{(\phi)}$ are given in (20) and (18). It worths noticing that, for the models here considered, the phase diffusion is dictated by the same relaxation time ruling the kinematic viscosity, i.e. fixed Schmidt number is considered. In order to decouple these two time scales a different more elaborated formulation based on multiple relaxation time schemes (MRT) [78,79] should be adopted.

2.2. The multicomponent free energy model

The other lattice Boltzmann variant that we consider in this work is the Free Energy (FE) based model [15–17]. Within this approach the equilibrium properties of the model are constructed to be consistent with an underlying continuum free energy functional of the order parameter, whose formulation is the following:

$$\mathcal{F}[\phi] = \mathcal{F}[\phi]_{id}+\mathcal{F}[\nabla\phi]_{nl} = \int\left[V(\phi)+\frac{\kappa}{2}|\nabla\phi|^2\right]d\mathbf{x}, \tag{26}$$

where $V(\phi)$ is the bulk free energy density and κ a constant parameter associated to the surface tension at the interface. The chemical potential $\mu(\phi)$ and the pressure tensor are derived from thermodynamics identities:

$$\mu(\phi) = \frac{\delta\mathcal{F}[\phi]}{\delta\phi} = \frac{\partial V(\phi)}{\partial\phi}-\kappa\Delta\phi, \tag{27}$$

$$\mathbf{P} = \left(P_b(\phi)-\kappa\phi\Delta\phi-\frac{\kappa}{2}|\nabla\phi|^2\right)\boldsymbol{\delta}+\kappa\nabla\phi\nabla\phi, \tag{28}$$

Please cite this article in press as: L. Scarbolo et al., Unified framework for a side-by-side comparison of different multicomponent algorithms: Lattice Boltzmann vs. phase field model, J. Comput. Phys. (2012), http://dx.doi.org/10.1016/j.jcp.2012.09.029

where $P_b(\phi) = \phi\partial V(\phi)/\partial\phi - V(\phi)$ is the bulk pressure. For the out of equilibrium properties, the mesoscopic dynamics is given by the following two coupled kinetic equations:

$$f_i(\mathbf{x}+\mathbf{c}_i\Delta t, t+\Delta t) - f_i(\mathbf{x},t) = -\frac{\Delta t}{\tau}[f_i(\mathbf{x},t) - f_i^{(eq)}(\rho,\phi,\mathbf{u})], \tag{29}$$

$$g_i(\mathbf{x}+\mathbf{c}_i\Delta t, t+\Delta t) - g_i(\mathbf{x},t) = -\frac{\Delta t}{\tau_g}[g_i(\mathbf{x},t) - g_i^{(eq)}(\phi,\mathbf{u})], \tag{30}$$

where the macroscopic density and velocity are given by:

$$\rho(\mathbf{x},t) = \sum_i f_i(\mathbf{x},t); \quad \mathbf{u}(\mathbf{x},t) = \frac{\sum_i f_i(\mathbf{x},t)\mathbf{c}_i}{\rho(\mathbf{x},t)}. \tag{31}$$

The order parameter density, ϕ, is obtained from the populations, g_i:

$$\phi(\mathbf{x},t) = \sum_i g_i(\mathbf{x},t). \tag{32}$$

The equilibrium distribution function is then chosen with a polynomial form in the kinetic velocities, so that:

$$\sum_i f_i^{(eq)}\mathbf{c}_i\mathbf{c}_i = \mathbf{P} + \rho\mathbf{u}\mathbf{u}, \tag{33}$$

$$\sum_i g_i^{(eq)}\mathbf{c}_i\mathbf{c}_i = \boldsymbol{\delta}\Gamma\mu + \phi\mathbf{u}\mathbf{u}, \tag{34}$$

where Γ controls the order parameter mobility $M = \Gamma(\tau_g - 1/2)$.[2] The previous kinetic model approximates the following macroscopic equations in the incompressible limit:

$$\frac{\partial\phi}{\partial t} + \nabla\cdot(\phi\mathbf{u}) = M\Delta\mu(\phi), \tag{35}$$

$$\rho\left(\frac{\partial\mathbf{u}}{\partial t} + \mathbf{u}\cdot\nabla\mathbf{u}\right) = -\nabla\cdot\mathbf{P} + \nabla\cdot(\eta(\tau)\nabla\mathbf{u} + \eta(\tau)\nabla\mathbf{u}^T), \tag{36}$$

where the viscosity is the same as in (25). The presence of extra spurious terms in the large scale expansions (35),(36) has been discussed in [80]. Through the numerical simulations presented in this work, these terms are directly evaluated and found to be negligibly small.

2.3. Matching in the long-wavelength limit

In this section the details of the matching between equations (24) and (25) and (35) and (36) are reported, representing the large scale limits of the SC and FE models, respectively, when compressible effects are negligible (ρ constant). Since the transport properties in the hydrodynamical equations are in fact the same, the crucial issue for the matching is to set the same thermodynamical background functional. First the continuity Eq. (24) is rewritten in a formulation similar to Eq. (35):

$$\frac{\partial\phi}{\partial t} + \nabla\cdot(\phi\mathbf{u}) = \nabla\cdot\mathbf{J}^{(\phi)} = \nabla[M(\phi)\nabla\mu], \tag{37}$$

where the chemical potential can be derived from the following $\tau-$dependent functional:

$$\mathcal{F}[\phi]^{(\tau)} = c_S^2\left(\frac{\rho+\phi}{2}\right)\log\left(\frac{\rho+\phi}{2}\right) + c_S^2\left(\frac{\rho-\phi}{2}\right)\log\left(\frac{\rho-\phi}{2}\right) + g_{AB}^{(\tau)}c_S^2\frac{(\rho^2-\phi^2)}{4} + \frac{g_{AB}^{(\tau)}c_S^4}{8}|\nabla\phi|^2, \tag{38}$$

from which, by definition, the chemical potential is extracted:

$$\mu^{(\tau)}(\phi) = \frac{\delta\mathcal{F}^{(\tau)}[\phi]}{\delta\phi} = \frac{\partial\mathcal{F}^{(\tau)}[\phi]}{\partial\phi} - \nabla\cdot\left[\frac{\partial\mathcal{F}[\phi]}{\partial(\nabla\phi)}\right] = \frac{c_S^2}{2}\log\left(\frac{\rho+\phi}{\rho-\phi}\right) - \frac{g_{AB}^{(\tau)}}{2}c_S^2\phi - \frac{g_{AB}^{(\tau)}}{4}c_S^4\Delta\phi, \tag{39}$$

and it coincides with Eq. (22). In order to set an accurate matching between the two lattice Boltzmann approaches, two more issues must be analyzed. Although one may think to integrate the FE model (29) and (30) with the functional (38) instead of (26), both continuity equations are not exactly the same due to the ϕ dependency of the mobility in Eq. (37). However, Eq. (37) can be approximated with the mobility in the center of the interface (that means negligibly small density changes $\phi \ll \rho$):[3]

[2] In the free energy approach the mobility can be easily changed by properly tuning both τ_g and Γ.

[3] Eq. (37) has been simulated with and without the constant mobility by adding proper counter-terms to the lattice Boltzmann equation. No substantial differences have been observed for the features analyzed in this paper.

Please cite this article in press as: L. Scarbolo et al., Unified framework for a side-by-side comparison of different multicomponent algorithms: Lattice Boltzmann vs. phase field model, J. Comput. Phys. (2012), http://dx.doi.org/10.1016/j.jcp.2012.09.029

$$M(\phi,\rho,\tau)\approx M(\rho,\tau)=\rho\left(\tau-\frac{1}{2}\right). \tag{40}$$

With this approximation, the advection–diffusion equation for the order parameter ϕ obtained from the SC model and from Eqs. (30) and (34) of the FE model with the functional (38) are set to be the same in the hydrodynamical limit. Furthermore the pressure tensor should be matched between the two (FE and SC) LBM descriptions. The functional of Eq. (38) contains a spurious and nonphysical τ dependence hidden inside the definition of $g_{AB}^{(\tau)}=(\tau g_{AB})/(\tau-1/2)$. Only towards the limit of large τ the functional (38) becomes independent of τ, whereas, for finite τ, this extra spurious dependency should be kept inside Eq. (38) in order to accurately match both SC and FE descriptions. This difference emerges in the SC model because the collisional kernel does not conserve momentum locally [13,14]. Therefore the lattice momentum should be shifted by a factor $\mathbf{F}\Delta t/2$ to reproduce the hydrodynamical equations. It is important to remark here that such a spurious contribution may be removed by curing the discrete forcing effects as described in [81]. This technique has already been adopted in recent simulations with the multicomponent SC model in the framework of the so-called multiple relaxation time schemes (MRT) [78,79].[4] Differently with respect to the chemical potential, the pressure tensor of the SC description can be directly extracted:

$$\mathcal{F}[\phi]=c_S^2\left(\frac{\rho+\phi}{2}\right)\log\left(\frac{\rho+\phi}{2}\right)+c_S^2\left(\frac{\rho-\phi}{2}\right)\log\left(\frac{\rho-\phi}{2}\right)+g_{AB}c_S^2\frac{(\rho^2-\phi^2)}{4}+\frac{g_{AB}c_S^4}{8}|\nabla\phi|^2=\mathcal{F}[\phi,\rho,\nabla\phi], \tag{41}$$

that is the large τ limit of (38). In fact, following standard procedures, the conserved current (pressure tensor) under the hypothesis of translational invariance of the free energy can be derived. The general expression is:

$$\mathbf{P}=-\mathcal{F}^{\lambda_1,\lambda_2}\boldsymbol{\delta}+\frac{g_{AB}c_S^4}{4}\nabla\phi\nabla\phi, \tag{42}$$

where the mass conserving free energy has been used:

$$\mathcal{F}^{\lambda_1,\lambda_2}[\phi,\rho,\nabla\phi]=\mathcal{F}[\phi,\rho,\nabla\phi]-\lambda_1\phi-\lambda_2\rho, \tag{43}$$

$\lambda_{1,2}$ are two Lagrange multipliers introduced to ensure the global conservation of ϕ and ρ. Their values are readily evaluated using the Euler–Lagrange equations (should be noticed that there are no gradients of ρ in the free energy functional):

$$\frac{\partial\mathcal{F}^{\lambda_1,\lambda_2}}{\partial\phi}=\nabla\cdot\left[\frac{\partial\mathcal{F}^{\lambda_1,\lambda_2}}{\partial(\nabla\phi)}\right],\frac{\partial\mathcal{F}^{\lambda_1,\lambda_2}}{\partial\rho}=\nabla\cdot\left[\frac{\partial\mathcal{F}^{\lambda_1,\lambda_2}}{\partial(\nabla\rho)}\right]=0, \tag{44}$$

this yields:

$$\lambda_1=\frac{\partial V(\phi,\rho)}{\partial\phi}-\frac{g_{AB}c_S^4}{4}\Delta\phi,\lambda_2=\frac{\partial V(\phi,\rho)}{\partial\rho}. \tag{45}$$

At the end, the following pressure tensor is obtained:

$$\mathbf{P}=\left[\phi\frac{\partial V(\phi,\rho)}{\partial\phi}+\rho\frac{\partial V(\phi,\rho)}{\partial\rho}-V(\phi,\rho)-\kappa\phi\Delta\phi-\frac{\kappa}{2}|\nabla\phi|^2\right]\boldsymbol{\delta}+\kappa\nabla\phi\nabla\phi, \tag{46}$$

where $\kappa=(c_S^4g_{AB})/4)$ and the bulk potential $V(\phi)$ given by:

$$V(\phi,\rho)=c_S^2\left(\frac{\rho+\phi}{2}\right)\log\left(\frac{\rho+\phi}{2}\right)+c_S^2\left(\frac{\rho-\phi}{2}\right)\log\left(\frac{\rho-\phi}{2}\right)+g_{AB}c_S^2\frac{(\rho^2-\phi^2)}{4}. \tag{47}$$

It can be immediately noticed:

$$\phi\frac{\partial V(\phi,\rho)}{\partial\phi}+\rho\frac{\partial V(\phi,\rho)}{\partial\rho}-V(\phi,\rho)=c_s^2\rho+c_S^2\frac{g_{AB}}{4}(\rho^2-\phi^2), \tag{48}$$

and, at the end:

$$\mathbf{P}=\left(c_s^2\rho+c_S^2\frac{g_{AB}}{4}(\rho^2-\phi^2)-\kappa\phi\Delta\phi-\frac{\kappa}{2}|\nabla\phi|^2\right)\boldsymbol{\delta}+\kappa\nabla\phi\nabla\phi, \tag{49}$$

that coincides with (18). We conclude that the momentum equation from the SC model and from Eqs. (29) and (33) of the FE model with the functional (41) are set to be the same in the hydrodynamical limit.

[4] Since the goal of the present work is to propose guidelines to match the SC and the FE approaches we limited the analysis to the basic versions of the algorithms.

Please cite this article in press as: L. Scarbolo et al., Unified framework for a side-by-side comparison of different multicomponent algorithms: Lattice Boltzmann vs. phase field model, J. Comput. Phys. (2012), http://dx.doi.org/10.1016/j.jcp.2012.09.029

3. The phase field model

In this section the phase field model for a multicomponent fluid system is analyzed. Starting from the features of the PFM proposed by Badalassi et al. [46] and Yue et al. [61], a new formulation of the free energy functional is derived to match the SC/FE multicomponent LBM reported in Section 2. For an isothermal binary mixture, where ϕ is the relative concentration of the mixture components, the free energy functional reads:

$$\mathcal{F}[\phi] = \mathcal{F}[\phi]_{id} + \mathcal{F}[\nabla\phi]_{nl} = \int \left[V(\phi) + \frac{\kappa}{2}|\nabla\phi|^2\right] \mathrm{d}\mathbf{x}, \tag{50}$$

where $V(\phi)$ is the ideal part of the specific free energy, $(\kappa/2)|\nabla\phi|^2$ is the non-local part of the specific free energy and κ is a constant positive parameter associated to the surface tension at the interface. Recalling Eq. (4) the chemical potential $\mu(\phi)$ is:

$$\mu(\phi) = \frac{\delta\mathcal{F}[\phi]}{\delta\phi} = \frac{\partial\mathcal{F}[\phi]}{\partial\phi} - \nabla\cdot\left[\frac{\partial\mathcal{F}[\phi]}{\partial(\nabla\phi)}\right] = \frac{\partial V(\phi)}{\partial\phi} - \kappa\Delta\phi. \tag{51}$$

For unsteady problems, the evolution of the system is described by the Cahn–Hilliard equation [47,48], in which the evolution of $\phi(\mathbf{x})$ in time is proportional to the gradient of the chemical potential:

$$\frac{\partial\phi}{\partial t} + \mathbf{u}\cdot\nabla\phi = \nabla\cdot[M(\phi,\rho,\tau)\nabla\mu(\phi)]. \tag{52}$$

According to Section 2.3, the functional chosen to describe the free energy of the system, is the τ-dependent $\mathcal{F}^{(\tau)}[\phi]$ of Eq. (38). Thus the chemical potential $\mu^{(\tau)}(\phi)$ reads:

$$\mu^{(\tau)}(\phi) = \frac{c_S^2}{2}\log\left(\frac{\rho+\phi}{\rho-\phi}\right) - \frac{g_{AB}^{(\tau)}}{2}c_S^2\phi - \frac{g_{AB}^{(\tau)}}{4}c_S^4\Delta\phi, \tag{53}$$

where the surface tension parameter is $\kappa = g_{AB}^{(\tau)}c_S^4/4$ and the coupling coefficient is $g_{AB}^{(\tau)} = (\tau g_{AB})/(\tau - 1/2)$. Substituting Eq. (53) for the chemical potential of Eq. (52) and considering the mobility parameter M uniform over the domain, the Cahn–Hilliard equation yields:

$$\frac{\partial\phi}{\partial t} + \mathbf{u}\cdot\nabla\phi = M(\rho,\tau)\Delta\mu^{(\tau)}(\phi). \tag{54}$$

Focusing on density-matched ($\rho \simeq$ const.), viscosity-matched ($\nu \simeq$ const.) and incompressible ($\nabla\cdot\mathbf{u} = 0$) Newtonian fluids, the flow field evolution is described by the modified Navier–Stokes equation [46]:

$$\frac{\partial\mathbf{u}}{\partial t} + \mathbf{u}\cdot\nabla\mathbf{u} = -\nabla p + \nu(\tau)\nabla\cdot(\nabla\mathbf{u} + \nabla\mathbf{u}^T) + \mathbf{F}_\phi, \tag{55}$$

where $\mathbf{F}_\phi$ is the local capillary stress due to the concentration field [82]. In order to match the same hydrodynamical properties of the multicomponent LBM, $\mathbf{F}_\phi$ is modeled according to the results of Section 2.3:

$$\mathbf{F}_\phi = \mu(\phi)\nabla\phi, \tag{56}$$

where $\mu(\phi)$ reads:

$$\mu(\phi) = \frac{c_S^2}{2}\log\left(\frac{\rho+\phi}{\rho-\phi}\right) - \frac{g_{AB}}{2}c_S^2\phi - \frac{g_{AB}}{4}c_S^4\Delta\phi. \tag{57}$$

Eq. (57) is obtained applying the definition (4) to the functional (41), which is derived from the matching procedure of Section 2.3. Within this formulation, $\mu(\phi)$ represents the large τ limit of the Eq. (53), and $\mu^{(\tau)} \to \mu$ when $\tau \gg 1/2$. Finally, the PFM equations implemented in this work are the following:

$$\nabla\cdot\mathbf{u} = 0, \tag{58}$$

$$\frac{\partial\phi}{\partial t} + \mathbf{u}\cdot\nabla\phi = M(\rho,\tau)\Delta\mu^{(\tau)}(\phi), \tag{59}$$

$$\frac{\partial\mathbf{u}}{\partial t} + \mathbf{u}\cdot\nabla\mathbf{u} = -\nabla p + \nu(\tau)\nabla\cdot(\nabla\mathbf{u} + \nabla\mathbf{u}^T) + \mu(\phi)\nabla\phi, \tag{60}$$

where the chemical potentials μ and $\mu^{(\tau)}$ are given by Eqs. (57) and (53) respectively. Their formulation is similar to that used by Mauri et al. [54], Vladimirova et al. [55] and Molin et al. [56]. The mobility coefficient of Eq. (59) is $M(\rho,\tau) = \rho(\tau - 1/2)$, whereas the kinematic viscosity of Eq. (60) reads $\nu(\tau) = c_S^2(\tau - 1/2)$. The coefficients τ, ρ, g_{AB} and $c_S^2 = 1/3$ are the LBM input parameters and their definitions are reported in Table 1. Eqs. (58)–(60) have been rewritten in a dimensionless form using the following dimensionless variables:

$$\mathbf{u}^- = \frac{\mathbf{u}}{U}, \quad \mathbf{x}^- = \frac{\mathbf{x}}{H}, \quad t^- = \frac{t}{H/U}, \quad p^- = \frac{p}{\rho U^2/H}, \quad \phi^- = \frac{\phi}{\phi^*}, \tag{61}$$

Please cite this article in press as: L. Scarbolo et al., Unified framework for a side-by-side comparison of different multicomponent algorithms: Lattice Boltzmann vs. phase field model, J. Comput. Phys. (2012), http://dx.doi.org/10.1016/j.jcp.2012.09.029

Table 1
Definition of the Lattice Boltzmann input parameters and of the corresponding phase field model dimensionless groups.

$\nu = c_S^2(\tau - \frac{1}{2})$	$M = \rho(\tau - \frac{1}{2})$	$\kappa = \frac{g_{AB}c_S^4}{4}$
$\beta = \frac{g_{AB}c_S^2}{2}$	$\beta^{(\tau)} = \frac{g_{AB}^{(\tau)}c_S^2}{2}$	$\xi = \sqrt{\frac{\kappa}{\beta}}$
$Pe = \frac{UH}{\beta^{(\tau)}M}$	$Ch = \frac{\xi}{H}$	$Ca = \frac{\nu\rho U}{\sqrt{\beta\kappa}}$
$Re = \frac{UH}{\nu^{(\tau)}}$		

Table 2
Definition of the Lattice Boltzmann and phase field input values.

ρ	τ	g_{AB}	$g_{AB}^{(\tau)}$	c_S^2
1.4	0.5	0.164	1.804	$\frac{1}{3}$
Pe	*Ch*	*Ca*	*Re*	
0.7930	0.0256	0.0021	1.000	

where H, U, ϕ^* are the characteristic length, velocity and concentration, respectively. Starting from Eq. (53), the chemical potential yields to:

$$\mu^-(\phi) = \frac{1}{G_{AB}} \log\left(\frac{\rho^- + \phi^-}{\rho^- - \phi^-}\right) - \phi^- - Ch^2\Delta\phi^-, \tag{62}$$

consistently Eq. (57) reads:

$$\mu^{(\tau)-}(\phi) = \frac{1}{G_{AB}^{(\tau)}} \log\left(\frac{\rho^- + \phi^-}{\rho^- - \phi^-}\right) - \phi^- - Ch^2\Delta\phi^-, \tag{63}$$

where $\rho^- = \rho/\phi^*, G_{AB} = g_{AB}\phi^*$ and $G_{AB}^{(\tau)} = g_{AB}^{(\tau)}\phi^*$. The dimensionless form of Eqs. (58)–(60) are:

$$\nabla\cdot\mathbf{u}^- = 0, \tag{64}$$

$$\frac{\partial\phi^-}{\partial t^-} + \mathbf{u}^-\cdot\nabla\phi^- = \frac{1}{Pe}\Delta\mu^{(\tau)-}, \tag{65}$$

$$\frac{\partial\mathbf{u}^-}{\partial t^-} + \mathbf{u}^-\cdot\nabla\mathbf{u}^- = -\nabla p^- + \frac{1}{Re}\nabla\cdot(\nabla\mathbf{u}^- + \nabla\mathbf{u}^{-T}) + \frac{1}{ReChCa}\mu^-\nabla\phi^-. \tag{66}$$

The non-dimensional groups introduced into the equations system (62)–(66) are the Cahn number, the Peclet number, the Reynolds number and the capillary number, which are defined as follows:

$$Ch = \frac{\xi}{H}, \quad Pe = \frac{UH}{\beta^{(\tau)}M}, \quad Re = \frac{UH}{\nu}, \quad Ca = \frac{\nu\rho U}{\sqrt{\beta\kappa}}. \tag{67}$$

The Cahn number is the ratio between the interface thickness ξ and the length-scale H, the Peclet number is the ratio between the diffusive time-scale $H^2/(\beta^{(\tau)}M)$ and the convective time-scale H/U. The Reynolds number is the ratio between the inertial forces HU and the viscous forces ν. Finally the capillary number is the ratio between the viscous forces $\nu\rho U$ and the capillary forces $\sqrt{\beta\kappa}$ at the interface. All the dimensionless groups and the definitions of the fluid properties with respect to the LBM input parameters are reported in Table 1. The equations system (62)–(66) can be easily extended to systems with different viscosity and different mobility between the two components [46]. Mismatched-density systems require the adoption of a density-based PFM [51].

3.1. The numerical method

The equations system (64)–(66) is directly solved using a pseudo-spectral algorithm in which the field variables are transformed into wave-number space by means of fast Fourier transform (FFT). The non-linear terms are evaluated in the physical space an then re-transformed into the wave-number space [83]. In order to reduce the time-step constraint required by the Cahn–Hilliard equation, an operator splitting technique has been introduced onto Eq. (65). The procedure adopted is similar to that discussed in [46] and it yields (where the apex "-" has been removed for sake of simplicity):

$$\frac{\partial\phi}{\partial t} = -\mathbf{u}\cdot\nabla\phi + \frac{1}{Pe}\Delta\left[\frac{1}{G_{AB}^{(\tau)}}\log\left(\frac{\rho+\phi}{\rho-\phi}\right) - 3\phi\right] - \frac{1}{Pe}\left(Ch^2 - \frac{\Delta t}{2Pe}\right)\Delta^2\phi + \frac{1}{Pe}\left[2\Delta^2\phi - \frac{\Delta t}{2Pe}\Delta^2\phi\right]. \tag{68}$$

Please cite this article in press as: L. Scarbolo et al., Unified framework for a side-by-side comparison of different multicomponent algorithms: Lattice Boltzmann vs. phase field model, J. Comput. Phys. (2012), http://dx.doi.org/10.1016/j.jcp.2012.09.029

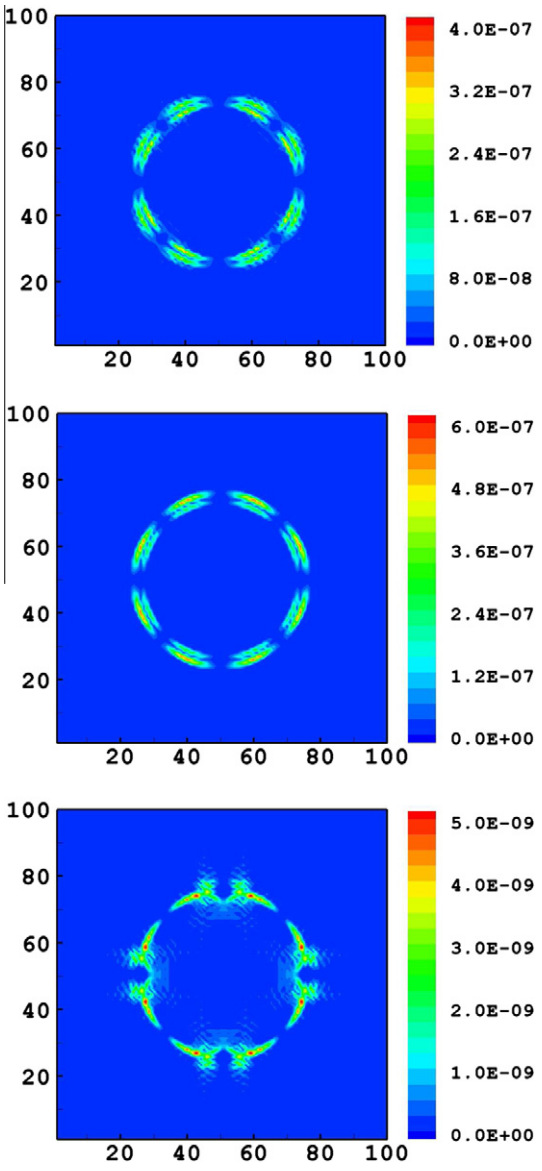

Fig. 1. Contour plots of the local kinetic energy, per unit density, $\frac{1}{2}(u_x^2+u_y^2)$ due to the spurious currents for the FE-LBM (top), SC-LBM (center) and PFM (bottom) methods when simulating a stationary two dimensional droplet. The snapshots are taken at the same time when a steady state has been attained. The intensity and structure of the spurious kinetic terms comparable in the lattice Boltzmann models and is reduced by a factor 100 in the PFM model (i.e. a factor 10 on the velocity magnitudes).

By explicit treatment of the first term on the right-hand-side of (68) and implicit treatment of the second term on the right-hand-side of Eq. (68), an efficient semi-implicit discretization is obtained. The time step advancement for both Eqs. (66) and (68) is obtained using a two-level Adams–Bashfort scheme for the explicit non-linear terms, and the Crank–Nicholson scheme for the implicit linear terms. Applied to Eq. (68) this implicit-explicit combination reads:

$$\frac{\phi^{n+1}-\phi^n}{\Delta t}=\frac{1}{2}\left(3S^n-S^{n-1}\right)+\frac{1}{2}\left(\Psi^{n+1}+\Psi^n\right), \tag{69}$$

where the explicit S term and the implicit Ψ term are:

$$S=-\mathbf{u}\cdot\nabla\phi+\frac{1}{Pe}\Delta\left[\frac{1}{G_{AB}^{(\tau)}}\log\left(\frac{\rho+\phi}{\rho-\phi}\right)-3\phi\right]-\frac{1}{Pe}\left(Ch^2-\frac{\Delta t}{2Pe}\right)\Delta^2\phi, \tag{70}$$

Please cite this article in press as: L. Scarbolo et al., Unified framework for a side-by-side comparison of different multicomponent algorithms: Lattice Boltzmann vs. phase field model, J. Comput. Phys. (2012), http://dx.doi.org/10.1016/j.jcp.2012.09.029

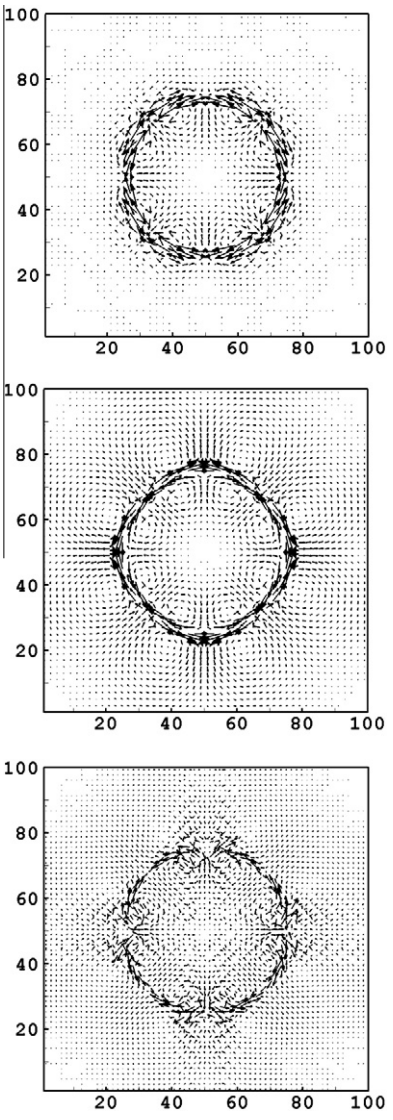

Fig. 2. Vector plots of the velocity field due to the spurious currents contributions for the FE-LBM (top), SC-LBM (center) and PFM (bottom) simulations for the two dimensional static droplet. The plots are taken at the same time when the steady state has been reached. The velocity field of the Lattice Boltzmann simulations (top and center plots) have been magnified by a factor 10^4 whereas the vector field of the PFM simulation have been magnified by a factor $5 \cdot 10^4$ for the sake of readability.

$$\Psi = \frac{1}{Pe}\left(2\nabla^2\phi - \frac{\Delta t}{2Pe}\nabla^4\phi\right). \tag{71}$$

More details on the numerical algorithm can be found in [83].

4. Numerical tests

In this section the numerical results obtained from both the PFM and the LBM approaches are discussed. Two different tests have been performed with the three models, SC-LBM, FE-LBM and PFM, as described in Sections 2.1, 2.2, and 3 respectively. First, the equilibration of a two dimensional static droplet has been simulated until the steady state has been reached. Then, starting from the settled droplet, its deformation under a Kolmogorov flow has investigate. For the numerical analysis a SC-LBM model with $\tau = 0.55$, $\rho = 1.4$ and $g_{AB} = 0.164$ has been used. The interaction parameter τ has been chosen small enough to avoid spurious contributions from the pressure tensor. The other parameters (g_{AB} and ρ) have been chosen in order to obtain $\phi = \rho_A - \rho_B = \pm 1$ inside the pure components. The simulations have been carried out on a two dimensional fully periodic grid of 100×100 nodes, on a computational domain of dimensions $L_x \times L_y = 100 \times 100$. The same simulations

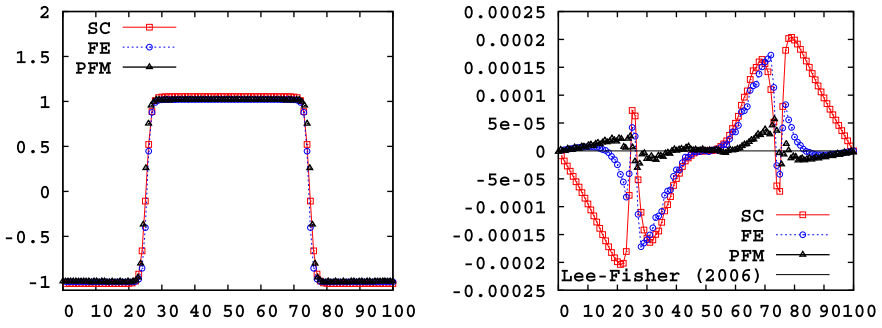

Fig. 3. Local concentration and velocity profiles from FE-LBM, SC-LBM and PFM simulations of a two dimensional static droplet. On the left the local order parameter, $\phi = \rho_A - \rho_B$, is plotted as a function of the coordinate, y, for fixed $x = 50$. On the right the local (spurious) velocity in the vertical direction, u_y, is plotted as a function of the coordinate, y, for fixed $x = 50$. The order of magnitude of both spurious contributions is comparable in the lattice Boltzmann models while is reduced by a factor 10 (for the velocity, 100 for energy) in the PFM model. Improvements in the LBM can be obtained by curing discretization errors in the computation of the intermolecular force as described by Lee and Fischer [67].

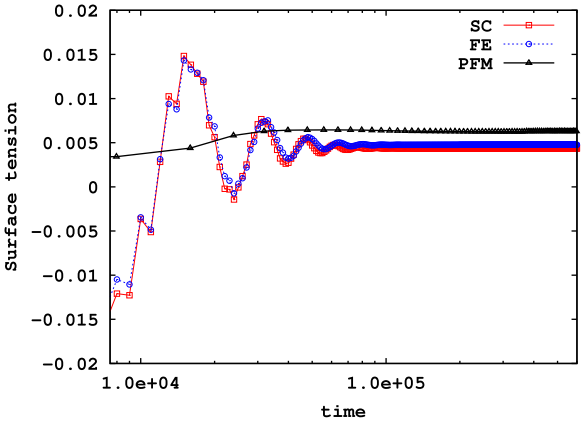

Fig. 4. Time evolution of the surface tension (Laplace test) from FE-LBM, SC-LBM and PFM simulations of a two dimensional static droplet. Starting from the same initial conditions, the local value of surface tension $\sigma(t)$ is plotted as a function of time.

performed with the SC model have been repeated with the FE-LBM. Then the PFM simulations have been performed on a two dimensional fully periodic grid[5] composed by 128×128 nodes on a computational domain of dimensions $L_x \times L_y = 2\pi H \times 2\pi H = 100 \times 100$. In particular, PFM dimensionless numbers have been calculated following the definitions reported in Table 1 and their values are collected in Table 2. In order to match $\phi = \pm 1$ in the regions of pure components, the scaling concentration parameter has been chosen $\phi^* = 1$. As result SC/FE-LBM and the phase field model have been set with the same interface and transport properties and thus the results can be both qualitatively and quantitatively compared.

4.1. A steady droplet

A two dimensional static droplet with radius approximately $R/L_x \simeq 1/4$ initiated in a resting fluid has been studied. The simulations have been run letting the drop attain a stationary, equilibrium state. The kinetic energy at the curved interface (Fig. 1) and and the associated stationary configuration of velocity field and order parameter (Figs. 2 and 3) have been measured. The spurious currents shown by the PFM simulations are found almost one order of magnitude smaller that the ones from the LBM. On the other hand both FE and SC LBM models show comparable velocity magnitudes. The flow fields patterns are similar within the three methods, even if in the PFM case these currents are confined in a thinner layer along the interface. Fig. 4 displays the temporal evolution of the surface tension σ, which is proportional to the difference between the pressure inside the drop (P_i) and the pressure outside the drop (P_o):

$$\sigma(t) = R[P_i(t) - P_o(t)]. \tag{72}$$

Both the left panel of Figs. 3 and 4 show that the interface properties of the three models are the same (i.e. the same interface structure and the same surface tension at the curved interface). Nevertheless, the oscillations observed in the LBM models in

[5] Due to the use of a spectral solver it is convenient to choose a power of 2 for the number of grid nodes.

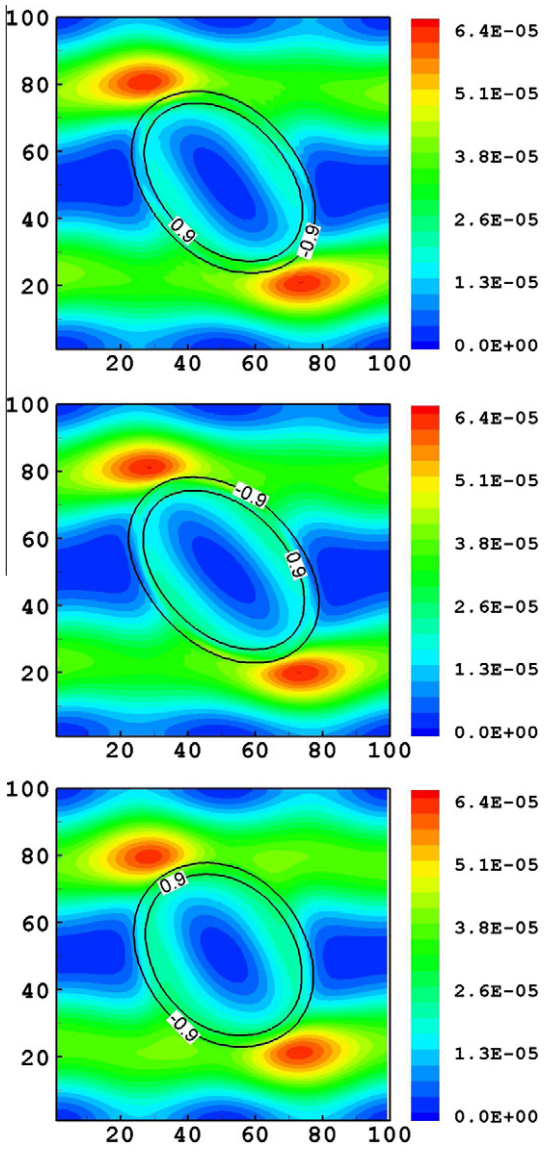

Fig. 5. Contour plot of the local kinetic energy per unit density $\frac{1}{2}(u_x^2 + u_y^2)$ for the FE-LBM (top), SC-LBM (center) and PFM (bottom) simulations of a two dimensional droplet deformation under Kolmogorov flow. The plots are taken at the same time when the steady state has been reached. Similar magnitudes and patterns can be observed for all the models.

Fig. 4 are probably nonphysical pressure fluctuations which are ruled out in the PFM simulations. The most important feature observed appears to be the change in magnitude and structure of spurious currents: in both the LBM simulations approximately the same spurious currents are found while their intensity is reduced in the case of PFM simulations. Nevertheless, it is important to remark that the LBM used here are basic versions of the two widely adopted approaches. Improvements can be obtained by curing discretization errors in the computation of the intermolecular force causing parasitic currents as described by Lee and Fischer [67]. Such improvements have been shown to eliminate currents to roundoff if the potential form of the intermolecular force is used with compact isotropic discretization. For the sake of completeness the results obtained with the Lee–Fischer scheme have been reported in Fig. 3.Fig. 5

4.2. Droplet deformation under Kolmogorov flow

Starting from the equilibrium droplet obtained from the simulation of Section 4.1, a sinusoidal forcing has been applied on the flow field until a new stationary state was reached. The forcing term has been chosen with the following formulation in order to generate a Kolmogorov flow:

Please cite this article in press as: L. Scarbolo et al., Unified framework for a side-by-side comparison of different multicomponent algorithms: Lattice Boltzmann vs. phase field model, J. Comput. Phys. (2012), http://dx.doi.org/10.1016/j.jcp.2012.09.029

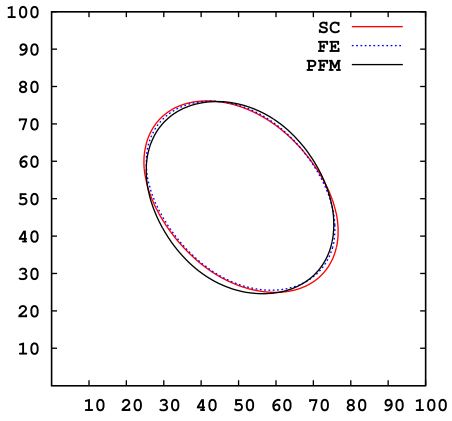

Fig. 6. Isocontour plot of the concentration field at $\phi = 0$ for the FE-LBM, SC-LBM and PFM model for a stationary two dimensional droplet under shear.

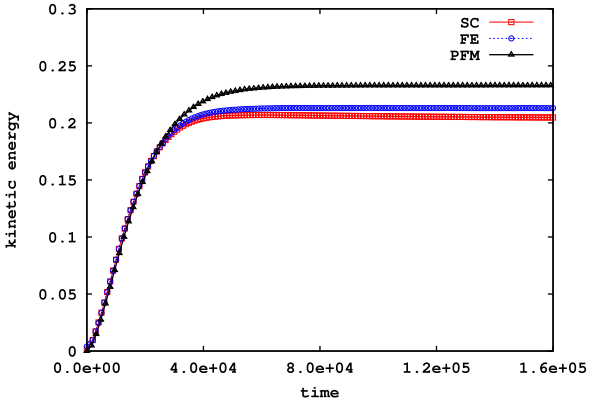

Fig. 7. Time evolution of the total kinetic energy from FE-LBM, SC-LBM and PFM simulations of a two dimensional droplet deformation under Kolmogorov flow. Starting from the same initial conditions, the total value of the kinetic energy $\iint (u_x^2 + u_y^2) \mathrm{d}x\mathrm{d}y$ is plotted as a function of time. Similar evolution in time is registered for all the models, even if the PFM showed an asymptotic value higher than the LBM. The CPU elapsed time of both PFM (T_{PFM}) and SC (T_{SC}) methods have been measured through this simulation. The Lattice Boltzmann method was roughly three times faster than the analogous phase field model ($\frac{T_{PFM}}{T_{SC}} = 2.9$).

$$F_x(\mathbf{x}) = \rho A \sin\left(\frac{2\pi y}{L_y}\right), \tag{73}$$

where $A = 10^{-6}$. In the PFM model the dimensionless forcing term is:

$$F_x^-(\mathbf{x}) = \frac{AH}{U^2} \sin\left(\frac{2\pi y}{L_y}\right). \tag{74}$$

The evolution of the total kinetic energy reported in the right panel of Fig. 7 shows a good matching between the three models, thus the same hydrodynamical transport properties have indeed been imposed. Little discrepancies (less than 10%) between PFM and LBM simulations are shown in the total kinetic energy of the steady state. Moreover little deformation differences can be observed for the concentration isocontours of Fig. 6, with the PFM showing a slightly less deformed drop with respect to both LBM. On the contrary both LBM models (SC and FE) show the same concentration profile. The differences in kinetic energy and deformation seem to be consistent one with the other, in fact the less deformed the droplet, the less energy is absorbed from the flow and thus the higher the total kinetic energy (for same external forcing). Qualitative snapshots of the kinetic energy are reported in Fig. 5, where the isocontours of $\phi = -0.9$ and $\phi = 0.9$ have been superposed to show the interfacial layer location. Similar patterns and magnitudes are observed within the three models, confirming the correct matching of the models. To test the importance of spurious mass flux across the interface, the mass leakage L has been monitored in time:Fig. 7

$$L(t) = \frac{M(t)}{M_0}, \tag{75}$$

Please cite this article in press as: L. Scarbolo et al., Unified framework for a side-by-side comparison of different multicomponent algorithms: Lattice Boltzmann vs. phase field model, J. Comput. Phys. (2012), http://dx.doi.org/10.1016/j.jcp.2012.09.029

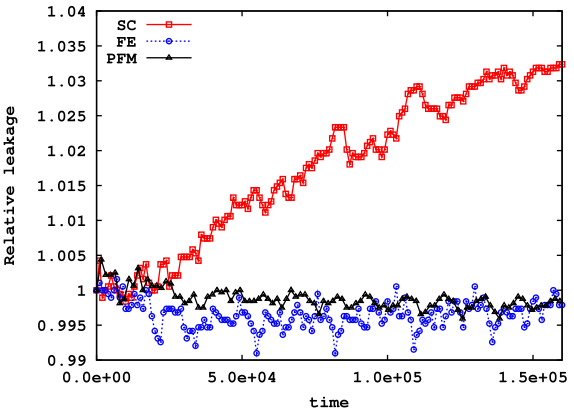

Fig. 8. Time evolution of the relative leakage of the order parameter from FE-LBM, SC-LBM and PFM simulations of a two dimensional droplet deformation under Kolmogorov flow. Starting from the same initial conditions, the relative leakage $L(t)$ is plotted as a function of time. Longer simulations show that the leakage reached the saturation value for all the three methods.

where $M(t)$ and M_0 are the number of computational nodes inside the droplet at time t and at time $t = 0$, respectively. The nodes with a local order parameter $\phi(\mathbf{x}) \geqslant \phi_T$, with $\phi_T = 0.0$, have been considered as belonging to the droplet. The results reported in Fig. 8 show a negligible mass leakage (less than 0.5%) for the PFM and FE, whereas it slightly higher (in the order of 1–3%) for SC-LBM.

5. Conclusions

In this work two of the most widely adopted approaches for the numerical study of multicomponent fluid systems, the Lattice Boltzmann models (LBM) and phase field models (PFM) have been compared on equal footing. First the Shan–Chen (SC) multicomponent LBM and the free energy (FE) LBM have been reviewed and analyzed. Focusing on the specific case of phase separating fluids with two species, the long-wavelength limit (i.e. the hydrodynamical limit) of both lattice Boltzmann models has been reviewed and a criteria to match the two models has been developed. Then, on the basis of the LBM matching, a new formulation for the free-energy involved into the PFM has been derived. In this way the analytical matching between PFM and LBM has been obtained. Finally the three models (SC-LBM, FE-LBM and PFM) have been numerically tested against controlled benchmarks with both steady and moving interfaces. Three main advantages emerge from this kind of analysis: first, from the theoretical point of view, it has been verified that the PFM equations are well approximated by the large scale limit of the multicomponent LBM. In fact, the convergence of the lattice Boltzmann models towards the diffuse-interface hydrodynamics may be questionable due to the presence of steep interfaces, where the local gradients are high enough to prevent the usual Chapman–Enskog analysis to be applied [20]. Second, from the computational viewpoint, some of the undesirable features emerging in the LBM simulations have been shown to exist also in the PFM, but these appear somewhat reduced, at least when basic versions of LBM are considered. Third, this study offers the possibility to test the performances of the different methods simulating the same physical system. The PFM shows a computational cost almost three times higher to the analogous LBM. On the other hand the quantitative results of a PFM appears to be more accurate. We believe this study helps clarify important issues beyond the choice of the either a lattice Boltzmann or a phase field based approaches for multicomponent fluid dynamics.

Acknowledgements

We thank L. Busolini for the help in the development of the phase field model algorithm. This work was carried out under the HPC-EUROPA2 project (Project No.: 228398), with the support of the European Community – Research Infrastructure Action of the FP7. This work is part of the research programme of the Foundation for Fundamental Research on Matter (FOM), which is part of the Netherlands Organisation for Scientific Research (NWO). We acknowledge the COST Action MP0806 for support. The research of the Udine group was also supported by the Italian Ministry for Research under the 2009 PRIN programme "Phase-field approach to chaotic mixing". M. Sbragaglia acknowledges support from DROEMU-FP7 IDEAS Contract No. 279004. We acknowledge computational support from SARA (NL), CINECA (IT) and Caspur (IT).

References

[1] E.P. Gross, E.A. Jackson, Kinetic models and the linearized Boltzmann equation, Phys. Fluids 2 (1959) 432.
[2] L. Sirovich, Kinetic modeling of gas mixtures, Phys. Fluids 5 (1962) 908.
[3] B.B. Hamel, Kinetic model for binary gas mixtures, Phys. Fluids 8 (1965) 418.
[4] B.B. Hamel, Two fluid hydrodynamic equations for a neutral, disparatemass, binary mixture, Phys. Fluids 9 (1966) 12.

Please cite this article in press as: L. Scarbolo et al., Unified framework for a side-by-side comparison of different multicomponent algorithms: Lattice Boltzmann vs. phase field model, J. Comput. Phys. (2012), http://dx.doi.org/10.1016/j.jcp.2012.09.029

[5] L. Sirovich, Mixtures of maxwell molecules, Phys. Fluids 9 (1966) 2323.
[6] S. Ziering, M. Sheinblatt, Kinetic theory of diffusion in rarefied gases, Phys. Fluids 9 (1966) 1674.
[7] E. Goldman, L. Sirovich, Equations for gas mixtures, Phys. Fluids 10 (1967) 1928.
[8] P.L. Bathnagar, E. Gross, M. Krook, A model for collision processes in gases. I. Small amplitude processes in charged and neutral one-component systems, Phys. Rev. 94 (1954) 511–525.
[9] L.S. Luo, S.S. Girimaji, Lattice Boltzmann model for binary mixtures, Phys. Rev. E 66 (2001) 035301.
[10] L.S. Luo, S.S. Girimaji, Theory of the lattice Boltzmann method: two-fluid model for binary mixtures, Phys. Rev. E 67 (2003) 036302.
[11] X. Shan, H. Chen, Lattice Boltzmann model for simulating flows with multiple phases and components, Phys. Rev. E 47 (1993) 1815–1819.
[12] X. Shan, H. Chen, Simulation of nonideal gases and liquid–gas phase-transitions by the lattice Boltzmann-equation, Phys. Rev. E 49 (1994) 2941–2948.
[13] X. Shan, G. Doolen, Multicomponent lattice-Boltzmann model with interparticle interaction, J. Stat. Phys. 81 (1995) 379–393.
[14] X. Shan, G. Doolen, Diffusion in a multicomponent lattice Boltzmann equation model, Phys. Rev. E 54 (1996) 3614.
[15] M.R. Swift, W.R. Osborn, J.M. Yeomans, Lattice Boltzmann simulation of nonideal fluids, Phys. Rev. Lett. 75 (1995) 830–833.
[16] A.J. Briant, A.J. Wagner, J.M. Yeomans, Lattice Boltzmann simulations of contact line motion. I. Liquid–gas systems, Phys. Rev. E 69 (2004) 031602.
[17] A.J. Briant, J.M. Yeomans, Lattice Boltzmann simulations of contact line motion. II. Binary fluids, Phys. Rev. E 69 (2004) 031603.
[18] X. Shan, Multicomponent lattice Boltzmann model from continuum kinetic theory, Phys. Rev. E 81 (2010) 045701.
[19] R. Benzi, S. Succi, M. Vergassola, The lattice Boltzmann-equation – theory and applications, Phys. Rep. 222 (1992) 145–197.
[20] D.A. Wolf-Gladrow, Lattice-gas Cellular Automata and Lattice Boltzmann Models, Springer, Berlin, 2000.
[21] S. Succi, The Lattice Boltzmann Equation for Fluid Dynamics and Beyond, Oxford University Press, 2005.
[22] S. Chen, G. Doolen, Lattice Boltzmann method for fluid flows, Annu. Rev. Fluid Mech. 30 (1998) 329–364.
[23] X. Shan, X.F. Yuan, H. Chen, Kinetic theory representation of hydrodynamics: a way beyond the Navier–Stokes equation, J. Fluid Mech. 550 (2006) 413–441.
[24] P.C. Philippi, L.A. Hegele, L.O.E. dos Santos, R. Surmas, From the continuous to the lattice Boltzmann equation: the discretization problem and thermal models, Phys. Rev. E 73 (2006) 056702.
[25] D.N. Siebert, L.A. Hegele, R. Surmas, L.O.E. Dos Santos, P.C. Philippi, Thermal lattice Boltzmann in two dimensions, Int. J. Mod. Phys. C 18 (2007) 546–555.
[26] X. Shan, X. He, Discretization of the velocity space in the solution of the Boltzmann equation, Phys. Rev. Lett. 80 (1998) 65–68.
[27] N.S. Martys, X. Shan, H. Chen, Evaluation of the external force term in the discrete Boltzmann equation, Phys. Rev. E 58 (1998) 6855–6857.
[28] J. Meng, Y. Zhang, Gauss–Hermite quadratures and accuracy of lattice Boltzmann models for nonequilibrium gas flows, Phys. Rev. E 83 (2011) 036704.
[29] X. Nie, X. Shan, H. Chen, Thermal lattice Boltzmann model for gases with internal degrees of freedom, Phys. Rev. E 77 (2008) 035701.
[30] S.S. Chikatamarla, I.V. Karlin, Lattices for the lattice Boltzmann method, Phys. Rev. E 79 (2009) 046701.
[31] S.S. Chikatamarla, I.V. Karlin, Entropy and Galilean invariance of lattice Boltzmann theories, Phys. Rev. Lett. 97 (2006) 190601.
[32] X. He, G. Doolen, Thermodynamic foundations of kinetic theory and Lattice Boltzmann models for multiphase flows, J. Stat. Phys. 107 (2001) 309–328.
[33] N.S. Martys, X. Shan, H. Chen, Evaluation of the external force term in the discrete Boltzmann equation, Phys. Rev. E 58 (1998) 6855–6857.
[34] X. He, X. Shan, G. Doolen, Discrete Boltzmann equation model for nonideal gases, Phys. Rev. E 57 (1998) R13–R16.
[35] P. Yuan, L. Schaefer, Equations of state in a lattice Boltzmann model, Phys. Fluids 18 (2006) 042101.
[36] A.L. Kupershtokh, D.A. Medvedev, D.I. Karpov, On equations of state in a lattice Boltzmann method, Comput. Math. Appl. 58 (2009) 965974.
[37] X. Shan, Pressure tensor calculation in a class of nonideal gas lattice Boltzmann models, Phys. Rev. E 77 (2008) 066702.
[38] J. Hyvaluoma, J. Harting, Slip flow over structured surfaces with entrapped microbubbles, Phys. Rev. Lett. 100 (2008) 246001.
[39] J. Zhang, F. Tian, A bottom-up approach to non-ideal fluids in the lattice Boltzmann method, Europhys. Lett. 81 (2008) 66005.
[40] R. Benzi, L. Biferale, M. Sbragaglia, S. Succi, F. Toschi, Mesoscopic modeling of a two-phase flow in the presence of boundaries: the contact angle, Phys. Rev. E 74 (2006) 021509.
[41] M. Sbragaglia, R. Benzi, L. Biferale, H. Chen, X. Shan, S. Succi, Lattice Boltzmann method with self-consistent thermo-hydrodynamic equilibria, J. Fluid Mech. 628 (2009) 299–309.
[42] R. Benzi, M. Sbragaglia, S. Succi, M. Bernaschi, S. Chibbaro, Mesoscopic lattice Boltzmann modeling of soft-glassy systems: theory and simulations, J. Chem. Phys. 131 (2009) 104903.
[43] A.J. Wagner, Thermodynamic consistency of liquid–gas lattice Boltzmann simulations, Phys. Rev. E 74 (2006) 056703.
[44] J.D. van der Waals, The thermodynamic theory of capillarity under the hypothesis of a continuous variation of density, J. Stat. Phys. 20 (1893) 200.
[45] V.V. Khatavkar, P.D. Anderson, H.E.H. Meijer, On scaling of diffuse-interface models, Chem. Eng. Sci. 61 (2006) 23.
[46] V.E. Badalassi, H.D. Ceniceros, S. Banerjee, Computation of multiphase systems with phase field model, J. Comput. Phys. 190 (2003) 371–397.
[47] J.W. Cahn, J.E. Hilliard, Free energy of a nonuniform system I, J. Chem. Phys. 28 (1958) 258.
[48] J.W. Cahn, J.E. Hilliard, Free energy of a nonuniform system III, J. Chem. Phys. 31 (1959) 688.
[49] D. Korteweg, Sur la forme que prennent les equations du mouvements des fluides si l'on tient compte des forces capillaires causees par des variations de densite considerables mais continues et sur la theorie de la capilarite dans l'hypothese d'une variation continue de la densite, Arch. Neerlandaises Sci. Exactes Nat. Ser. II 6 (1901) 1–21.
[50] D. Jacqmin, Calculation of two-phase Navier–Stokes flows using phase field modelling, J. Comput. Phys. 155 (1999) 96–127.
[51] J. Lowengrub, L. Truskinovsky, Quasi-incompressible Cahn Hilliard fluids, Proc. R. Soc. Lond. Ser. A 454 (1998) 2617–2654.
[52] K. Kawasaki, Kinetic equations and time correlation functions of critical fluctuations, Ann. Phys. 61 (1970) 1–56.
[53] P.C. Hohenberg, B.I. Halperin, Theory of dynamic critical phenomena, Rev. Mod. Phys. 49 (3) (1977) 435.
[54] R. Mauri, R. Shinnar, G. Triantafyllou, Spinodal decomposition in binary mixtures, Phys. Rev. E 53 (1996) 2613–2623.
[55] N. Vladimirova, A. Mangoli, R. Mauri, Diffusion-driven phase separation of deeply quenched mixtures, Phys. Rev. E 58 (1998) 7691–7699.
[56] D. Molin, R. Mauri, Enhanced heat transport during phase separation of liquid binary mixtures, Phys. Fluids 19 (2007) 074102.
[57] D. Molin, R. Mauri, Spinodal decomposition of binary mixtures with composition-dependent heat conductivities, Chem. Eng. Sci. 63 (2008) 2402–2407.
[58] A.G. Lamorgese, R. Mauri, Nucleation and spinoidal decomposition of liquid mixtures, Phys. Fluids 17 (2005) 034107.
[59] D.M. Anderson, G.B. McFadden, Diffuse-interface methods in fluid mechanics, Annu. Rev. Fluid. Mech. 30 (1998) 139–165.
[60] C. Liu, J. Shen, A phase field model for the mixture of two incompressible fluids and its approximation by a Fourier-spectral method, Physica D 179 (2003) 211–228.
[61] P. Yue, J.J. Feng, C. Liu, J. Shen, A diffuse-interface method for simulating two-phase flows of complex fluids, J. Fluid Mech. 515 (2004) 293–317.
[62] D. Jacqmin, Contact-line dynamics of a diffuse fluid interface, J. Fluid Mech. 402 (2000) 57–88.
[63] P. Yue, C. Zhou, J.F. Shen, Sharp-interface limit of the Cahn Hilliard model for moving contact lines, J. Fluid Mech. 645 (2010) 279–294.
[64] Z. Guo, C. Zheng, B. Shi, Force imbalance in lattice Boltzmann equation for two-phase flows, Phys. Rev. E 83 (2011) 036707.
[65] A. Cristea, V. Sofonea, Reduction of spurious velocity in finite difference lattice Boltzmann models for liquid–vapor systems, Int. J. Mod. Phys. C 14 (2003) 1251–1266.
[66] A.J. Wagner, The origin of spurious velocities in lattice Boltzmann, Int. J. Mod. Phys. B 17 (2003) 193–196.
[67] T. Lee, P.F. Fischer, Eliminating parasitic currents in the lattice Boltzmann equation method for nonideal gases, Phys. Rev. E 74 (2006) 046709.
[68] X. Shan, Pressure tensor calculation in a class of nonideal gas lattice Boltzmann models, Phys. Rev. E 77 (2008) 066702.
[69] M. Sbragaglia, R. Benzi, L. Biferale, S. Succi, K. Sugiyama, F. Toschi, Generalized lattice Boltzmann method with multirange pseudopotential, Phys. Rev. E 75 (2007) 026702.
[70] D. Jamet, D. Torres, J.U. Brackbill, On the theory and computation of surface tension: the elimination of parasitic currents through energy conservation in the second-gradient method, J. Comput. Phys. 182 (2002) 262–276.

Please cite this article in press as: L. Scarbolo et al., Unified framework for a side-by-side comparison of different multicomponent algorithms: Lattice Boltzmann vs. phase field model, J. Comput. Phys. (2012), http://dx.doi.org/10.1016/j.jcp.2012.09.029

[71] Y. Renardy, M. Renardy, PROST: a parabolic reconstruction of surface tension for the volume-of-fluid method, J. Comput. Phys. 183 (2002) 400–421.
[72] R. Scardovelli, S. Zaleski, Direct numerical simulation of free-surface and interfacial flow, Annu. Rev. Fluid Mech. 31 (1999) 567–603.
[73] S. Arcidiacono, I.V. Karlin, J. Mantzaras, C.E. Frouzakis, Lattice Boltzmann model for the simulation of multicomponent mixtures, Phys. Rev. E 76 (2007) 046703.
[74] P. Asinari, Lattice Boltzmann scheme for mixture modeling: Analysis of the continuum diffusion regimes recovering Maxwell–Stefan model and incompressible Navier–Stokes equations, Phys. Rev. E 80 (2009) 056701.
[75] X. Shan, Multicomponent lattice Boltzmann model from continuum kinetic theory, Phys. Rev. E 81 (2010) 045701.
[76] J. Kim, J. Lowengrub, Phase field modeling and simulation of three-phase flows, Interf. Free Bound. 7 (2005) 435–466.
[77] J. Park, R. Mauri, P.D. Anderson, Phase separation of viscous ternary liquid mixtures, Chem. Eng. Sci. 80 (2012) 270–278.
[78] Z.H. Chai, T.S. Zhao, A pseudopotential-based multiple-relaxation-time lattice Boltzmann model for multicomponent/multiphase flows, Acta Mech. Sin. 28 (2012) 983–992.
[79] Z. Yu, H. Yang, L.S. Fan, Numerical simulation of bubble interactions using an adaptive lattice Boltzmann method, Chem. Eng. Sci. 66 (2011) 3441–3451.
[80] V. Kendon, M. Cates, I. Pagonabarraga, J.C. Desplat, P. Blandon, Inertial effects in three-dimensional spinodal decomposition of a symmetric binary fluid mixture: a lattice Boltzmann study, J. Fluid Mech. 440 (2001) 147–203.
[81] Z. Guo, C. Zheng, B. Shi, Discrete lattice effects on the forcing term in the lattice Boltzmann method, Phys. Rev. E 83 (2002) 046308.
[82] E.B. Naumann, D.Q. He, Nonlinear diffusion and phase separation, Chem. Eng. Sci. 56 (2001) 1999–2018.
[83] A. Soldati, S. Banerjee, Turbulence modification by large-scale organized electrohydrodynamic flows, Phys. Fluids 10 (1998) 1742–1756.

Please cite this article in press as: L. Scarbolo et al., Unified framework for a side-by-side comparison of different multicomponent algorithms: Lattice Boltzmann vs. phase field model, J. Comput. Phys. (2012), http://dx.doi.org/10.1016/j.jcp.2012.09.029